Received 23 August 2024; revised 20 September 2024; accepted 24 September 2024. Date of publication 30 September 2024; date of current version 30 January 2025.

Digital Object Identifier 10.1109/OJAP.2024.3470209

A Hybrid Frequency Selective Absorber With Dual-Polarized Wireless Communication and Ultra-Wideband Absorption

YOUQUAN WEN[1], SAI-WAI WONG[1] (Senior Member, IEEE), CHUNLIN JI[2], RUOPENG LIU[2], AND YEJUN HE[1] (Senior Member, IEEE)

[1]State Key Laboratory of Radio Frequency Heterogeneous Integration, College of Electronics and Information Engineering, Shenzhen University, Shenzhen 518060, China

[2]State Key Laboratory of Metamaterial Electromagnetic Modulation Technology, Kuang-Chi Institute of Advanced Technology, Shenzhen 518000, China

CORRESPONDING AUTHOR: S.-W. WONG (e-mail: wongsaiwai@ieee.org)

This work was supported in part by the National Natural Science Foundation of China under Grant 62171289; in part by the State Key Laboratory of Radio Frequency Heterogeneous Integration (Independent Scientific Research Program) under Grant 2024012; and in part by the State Key Laboratory of Metamaterial Electromagnetic Modulation Technology, Kuang-Chi Institute of Advanced Technology, Shenzhen, China.

ABSTRACT Traditional multi-layer frequency selective absorbers (FSAs) with antenna circuit suffer from inter-layer interference, which can adversely affect the in-band frequency bandwidth of wireless communication (fractional bandwidth FBW <20% in literature). In this paper, a circuit design of decoupling between FSA-layer and antenna layer is proposed to solve this problem. The hybrid FSA with antenna circuit achieves in-band wideband dual-polarized transmitting/receiving and ultra-wideband absorption of both in-band and out-of-band. The two circuit layers operate independently, resolving the problems of inter-layer interference of conventional multi-layer FSA with antenna circuit. Additionally, the antenna configuration allows for excitation at the receiving end, providing broadband radiation capability without affecting in-band absorption. A prototype of the proposed structure is fabricated with a low profile of $0.22\lambda_0$. Simulated and measured results demonstrate the in-band FBW of 65.06% for wireless communication (2.8–5.5 GHz which is much wider than those reported FSAs with antenna circuit, e.g., FBW<20%) for two polarizations, with isolation less than −15 dB. Furthermore, the structure achieves impressive absorption performance, with radar cross-section reduction (RCSR) of 10 dB from 2.8 to 23 GHz (FBW=156.6%), and stable basic RCSR up to an oblique incidence of 30°.

INDEX TERMS Frequency-selective-absorber, radar cross section reduction, ultra-wideband absorption.

I. INTRODUCTION

FREQUENCY selective absorbers (FSAs) have attracted significant attention in military and civil fields, which are commonly employed in platform for low radar cross-section (RCS) application [1], [2], [3], [4]. FSAs originate from the initial Jaumann absorbers [5], [6] to circuit analog absorbers [7], [8], [9], multilayer FSA structures [10], [11], [12], and even more complex three-dimensional (3-D) FSA structures [13], [14], [15]. In [16], a special method is proposed for designing an ultra-wideband (UWB) absorber structure, termed as the antenna-based absorber. This structure incorporates planar dipole array with absorbing feeds. According to the reciprocity theorem of antenna [17], incident waves pass through the receiving antenna arrays, ultimately being absorbed by resistors connected at feeding port. By designing the array structure reasonably and adjusting the parameters of the absorbing feeds, it achieves a wider absorption bandwidth within the operating frequency band. Subsequently, other types of UWB antenna-based absorber were proposed, such as tightly coupled arrays [18], [19], [20], [21], [22]. The absorption characteristics, broadband performance, and angular stability of FSA have been significantly enhanced through these advancements. However, these methods merely adapt the wideband antenna structure into an FSA but lack of radiation functionality, failing to meet the demands of scenarios requiring both stealth and

© 2024 The Authors. This work is licensed under a Creative Commons Attribution-NonCommercial-NoDerivatives 4.0 License.
For more information, see https://creativecommons.org/licenses/by-nc-nd/4.0/

communication capabilities in practical applications. In the integrated design with antenna circuits, these methods often sacrifice absorption bandwidth, thus limiting their overall performance [23].

The aforementioned works only proposed single FSA function, which does not meet the wireless communication requirement. Currently, common FSAs with antenna function can absorb electromagnetic waves within specific frequency ranges while allowing transmission or reflection of electromagnetic waves, called absorptive frequency selective reflectors (AFSRs) [24], [25] and the absorptive frequency selective transmitters (AFSTs) [26]. However, these integrated designs have some challenges. For in-band waves, the absorption band of FSA overlaps with the operating frequency band of antenna. It can cause conflicts between absorption and radiation. In this condition, the FSA may affect radiation efficiency and bandwidth. Several methods such as employing polarization rotation reflective surfaces (PRRS) to separate co-polarized and cross-polarized waves or using diodes to switch between radiation and absorption modes, are commonly utilized, as described in [27], [28], [29], [30], [31], [32]. Nevertheless, when FSA integrates with antenna function, a trade off among two functions will limit both the FSA and antenna performance. Particularly, the bandwidth of antenna will be limited due to the inter-layer interference among two function layers [33]. Thus, an FSA with wideband antenna function (e.g., FBW>20% for wireless communication) is not reported in literature.,

In this paper, a circuit design of decoupling between FSA-layer and antenna layer is proposed to solve the problem of narrow frequency band for wireless communication of hybrid FSA with antenna circuit. Its novel design features an integrating antenna-based absorber enabling the structure to receive incoming waves and subsequently absorb them at the feeding port. By modifying the feeding network of the central 2×2 array region to serve as excitation ports, it maintains the ability of antenna radiation and in-band absorption, simultaneously. Besides, an FSA-layer is added in the structure for absorbing out-of-band waves. Besides, the hybrid structure achieves an attractive function of both in-band and out-of-band RCS reduction, which is hard to find in literature. This structure demonstrates promising potential for dual-function and multi-application across various radar systems and communication devices with wideband properties for both dual-polarized radiation (FBW=65.06%) and absorption (FBW=156.6%).

II. GEOMETRY AND OPERATING PRINCIPLE

Fig. 1 illustrates the schematic model of the proposed hybrid FSA with antenna circuit. The proposed hybrid FSA is composed by patch-layer, pillars, FSA-layer, and feed-layer. As shown in Fig. 1, in-band incident waves pass through, ultimately be absorbed by the resistors in feed-layer. Besides, out-of-band wave are absorbed by the FSA-layer. For radiation, electromagnetic waves are excited by feeding ports and coupled through the aperture to the pillars and patch-layer,

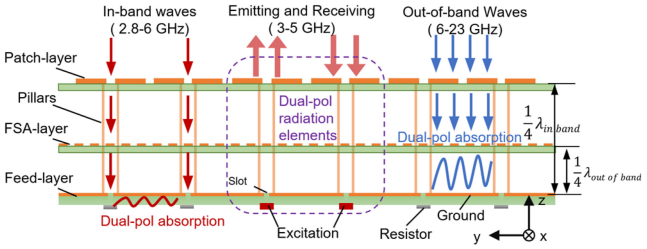

FIGURE 1. Schematic model of the proposed hybrid FSA with antenna circuit (Section view of yoz).

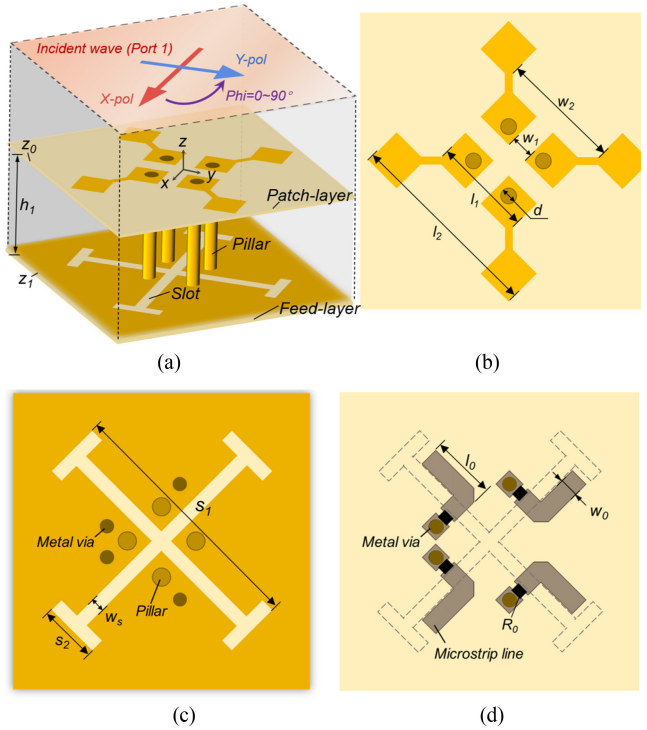

FIGURE 2. Unit cell of antenna-based FSA. (a) 3-D view of the model, (b) Top view of the patch-layer, (c) Top view of the feed-layer, (d) Bottom view of the feed-layer. (Structure parameters: $h_1 = 15$, $p_1 = 41.6$, $w_1 = 3$, $w_2 = 17$, $l_1 = 12$, $l_2 = 26$, $d = 3$, $s_1 = 31$, $s_2 = 7$, $w_s = 1.2$, $w_0 = 2.8$, $l_0 = 17.87$, all in mm; $R_0 = 50\ \Omega$).

which act as ME-dipole arrays. The central 2×2 elements are connected to an excitation port, while remaining elements are connected to the absorbing feeds. Therefore, it achieves wideband radiation with dual-polarization characteristics, in-band and out-of-band absorption simultaneously.

III. DESIGN OF THE ANTENNA-BASED ABSORBER

For in-band incident waves, Fig. 2 illustrates the unit cell of the antenna-based absorber, along with the corresponding parameters. The proposed FSA designs symmetrical patterns along the x-axis and y-axis. In Fig. 2 (a), the proposed FSA comprises the patch-layer, pillars, and the feed-layer. The vertical copper pillars are mounted between the patch-layer and the feed-layer through metal vias. The height of vertical copper pillars is denoted as h_1. When Port 1 acts as the incident wave from free space, the polarization direction of the incident wave varies with the angle *Phi*. It is

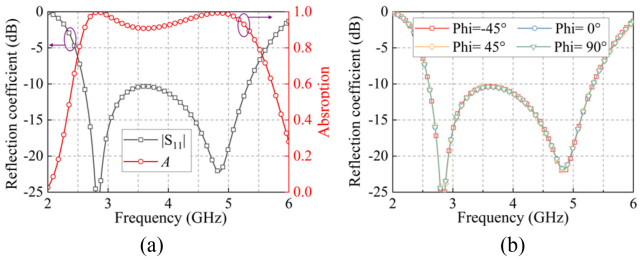

FIGURE 3. Simulated results of unit cell of antenna-based FSA. (a) |S11| and Absorption, (b) reflection coefficients for different Phi incident waves.

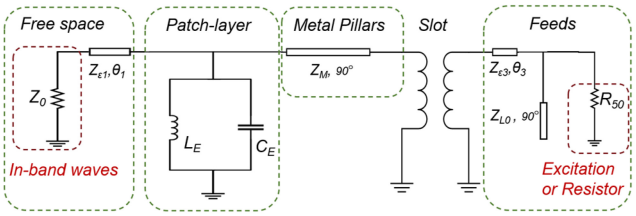

FIGURE 4. Equivalent circuit model of the antenna-based FSA. (Circuit parameters: $C_1 = 0.048$ pF, $L_1 = 36.5$ nH, $R_{50} = 50\ \Omega$, $Z_{\varepsilon 1} = 135$, $\theta_1 = 90$, $Z_m = 120$, $Z_{\varepsilon 3} = 82$, $\theta_3 = 90$, $Z_{L0} = 50$).

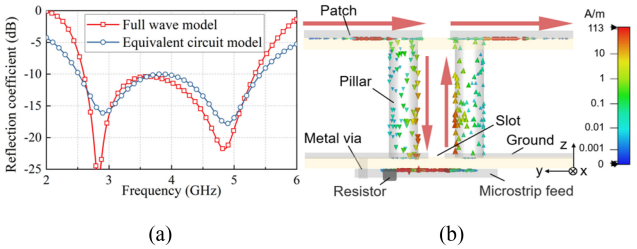

FIGURE 5. (a) Comparison results of the antenna-based FSA for ECM and full wave simulation, (b) The current distribution of unit cell structure of antenna-based FSA at 4 GHz.

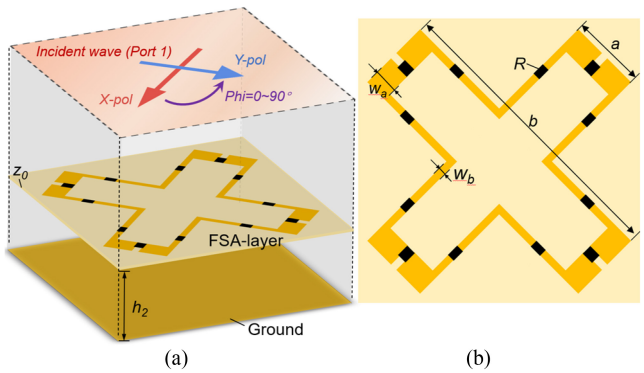

FIGURE 6. Unit cell of the FSA-layer with ground. (a) 3-D view of the model, (b) Top view. (Structure parameters: $h_2 = 5$, $p_2 = 10.4$, $w_a = 2.7$, $w_b = 0.3$, a = 1.4, $b = 11.8$, all in mm; $R = 60\ \Omega$.)

noteworthy that the x- and y-polarized waves correspond to $Phi = 0°$ and $Phi = 90°$, which is parallel to the diagonal of the unit cell, respectively. As shown in Fig. 2(b), the patch-layer consists of four symmetrical patches, which is printed on F4BM substrates with the thickness of $z_0 = 0.25$ mm and the relative permittivity of $\varepsilon_r = 2.65$. The dumbbell-shaped design aims for miniaturization [34]. In Fig. 2 (c), the front view of the feed-layer is designed as a Jerusalem-shaped metal slot, enabling in-band incident waves to enter the feeding network while reflecting out-of-band incident waves. In Fig. 2 (d), the bottom side of the feed-layer shows a feeding network connected to resistors, facilitating the absorption of in-band waves. It is also printed on F4BM substrates with the thickness of $z_1 = 1$ mm. Fig. 3 presents the reflection coefficient results of the antenna-based absorber. It is noteworthy that when the incident wave is set as port 1 and the other port is grounded, the relationship between $|S_{11}|$ and the absorption A can be expressed by the formula ($A = 1 - |S_{11}|^2$) [35]. In Fig. 3 (a), the reflection coefficient is less than -10 dB in the frequency range of 2.6-5.3 GHz, indicating the absorption exceeding 90%. Fig. 3 (b) illustrates the reflection coefficient when port 1 is exposed to incident waves at different Phi angles ($Phi = -45°$, $0°$, $45°$, $90°$) from free space. It can be indicated that the reflection coefficients for different polarized incident waves are stable.

To illustrate the functionality of the antenna-based absorber, Fig. 4 depicts the corresponding equivalent circuit model (ECM) [19]. Due to its symmetrical unit cell, the following analysis of ECM can be uniformly regarded as x-polarized incident waves. As shown in the ECM, the in-band wave from free space is equivalent to a transmission line with a characteristic impedance of Z_0. And the impedance of the dielectric substrate can be denoted to $Z_{\varepsilon 1}$ and $Z_{\varepsilon 2}$. The patch-layer can be approximated as an LC parallel resonant circuit, where the inductor L_E represents inductance of the patch, and the capacitor C_E denote the gap between the adjacent patches. The characteristic impedance of Z_e and Z_m can be determined by the formula [36]:

$$Z_e = \sqrt{\frac{L_e}{C_e}} \tag{1}$$

$$Z_m = \frac{1}{2} Z_d = \frac{60}{\sqrt{\varepsilon_r}} arcosh\left(\frac{D_r}{2r_0}\right) \tag{2}$$

where ε_r is the relative permittivity, D_r is the center spacing of two adjacent copper pillars, and r_0 is the diameter of the copper pillar. The slot on the frontside of the feed-layer is equivalent to a transformer. And the feeds on the backside of the feed-layer can be denoted as the matching circuit of microstrip lines with the impedance of Z_{L1} and Z_{L2}. The end of feeds is connected in parallel with the resistor of R_{50}. By adjusting the values of circuit parameters, two resonant frequencies can be achieved, enabling the structure to have wideband absorption at operating frequency. Fig. 5 (a) illustrates the comparison of reflection coefficients between ECM simulated result and full-wave simulated result, which has a good agreement for both cases. In addition, the current distribution at 4 GHz is given in Fig. 5 (b). The current is distributed at the surface of the patches, inside of pillars and concentrated in the microstrip feed

connected with the surface mounted resistor. This current distribution suggests that the patches and pillars act as a ME-dipole to enhance the bandwidth of antenna-based absorber [37].

IV. DESIGN OF THE FSA-LAYER

For out-of-band waves, the model of the FSA-layer at the boundary conditions of the unit cell is presented in Fig. 6. It is designed as a periodic structure of cross-ring shape, loaded with series resistors. In Fig. 6 (b), It is noteworthy that unit cell is 1/4 size of antenna-based absorber, allowing the FSA-layer to smoothly pass low-frequency waves (in-band) while absorbing high-frequency waves (out-of-band). Fig. 7(a) present the reflection coefficient of the FSA-layer. It can be observed that the reflection coefficient results in the frequency range of 6-23 GHz are less than −10 dB, indicating an energy absorption rate exceeding 90%. Fig. 7 (b) provides the reflection coefficient and transmission coefficient simulation results of the FSA-layer without ground. It can be observed that the transmission coefficient of the incident waves in the frequency range of 2-6 GHz is relatively high, suggesting the allowance of low-frequency waves (in-band) to pass through. Fig. 7 (c) shows the reflection coefficient with different resistances of R. It can be noted that by varying the resistance value, one can control the impedance conditions of FSA, and when $R = 60\ \Omega$, the FSA-layer exhibits the absorption FBW of 117.2%. Fig. 7 (d) illustrates the reflection coefficient when port 1 is exposed to incident waves at different *Phi* angles from free space. Because of the symmetrical patterns, it is evident that the reflection coefficients for different polarized incident waves remain stable. Furthermore, the ECM of the FSA-layer are presented in Fig. 8 (a) [38]. In the model, the transmission lines of Z_0 can be regarded as the wave transmission in free space, the dielectric substrate and the distance between FSA-layer and ground. The left and right sides of the cross-ring can be simplified as an RLC series circuit of R_1L_1 and C_1, and a parallel connection of R_3 and C_3 (corresponding to the edge effect of FSA-layer). While the center sides of the cross-ring can be simplified as an RLC series circuit of R_2L_2 and C_2. And the transmission line of $Z_{\varepsilon 1}$and $Z_{1/4}$ can respectively be equal to the thin substrate and the height of h_2 between FSA-layer and ground. For the ECM shown in Fig. 8(b), it can be obtained the reflection coefficient Γ as follows:

$$\Gamma = \frac{Z_{in} - Z_0}{Z_{in} + Z_0} = \frac{Y_0 - Y_{in}}{Y_0 + Y_{in}} \tag{3}$$

$$Y_{in} = Y_0 + Y_1 + Y_2 + Y_d \tag{4}$$

where characteristic admittance of each part as follows [8]:

$$Y_1 = \frac{1}{Z_{RLC1} + Z_{RC3}} = \frac{1}{R_1 + j\left(\omega L_1 - \frac{1}{\omega C_1}\right) + R_3 + \frac{1}{j\omega C_3}} = G_1 + jB_1 \tag{5}$$

$$Y_2 = \frac{1}{R_2 + j\left(\omega L_2 - \frac{1}{\omega C_2}\right)} = G_2 + jB_2 \tag{6}$$

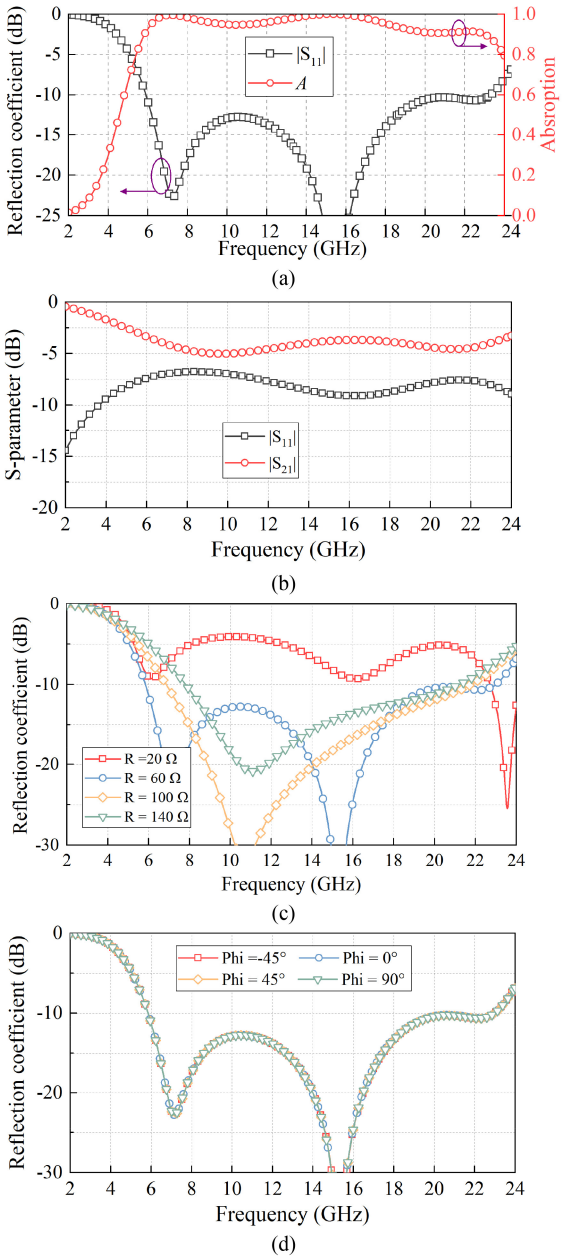

FIGURE 7. Simulated results of the FSA-layer with ground. (a) $|S_{11}|$ and Absorption, (b) $|S_{11}|$ and $|S_{21}|$ of FSA-layer without ground, (c) reflection coefficients for different *R*, (d) reflection coefficients for different Phi incident waves.

$$Y_d = j\frac{Y_{\varepsilon 1}\left(Y_{\varepsilon 1}\tan(\beta_0 h_0) - Y_{1/4}\cot(\beta_1 h_1)\right)}{Y_{\varepsilon 1} + Y_{1/4}\cot(\beta_1 h_1)\tan(\beta_0 h_0)} = jB_d \tag{7}$$

where $\beta_0 = 2\pi\sqrt{\varepsilon_1}/\lambda$, $\beta_1 = 2\pi/\lambda$, $\omega = 2\pi f$, thus the real and imaginary parts separately as follows:

$$G_1 = \frac{R_1}{R_1^2 + \left(\omega L_1 - \frac{1}{\omega C_1}\right)^2} + \frac{1}{R_3} \tag{8}$$

$$B_1 = \frac{\left(\omega L_1 - \frac{1}{\omega C_1}\right)}{R_1^2 + \left(\omega L_1 - \frac{1}{\omega C_1}\right)^2} + \omega C_3 \tag{9}$$

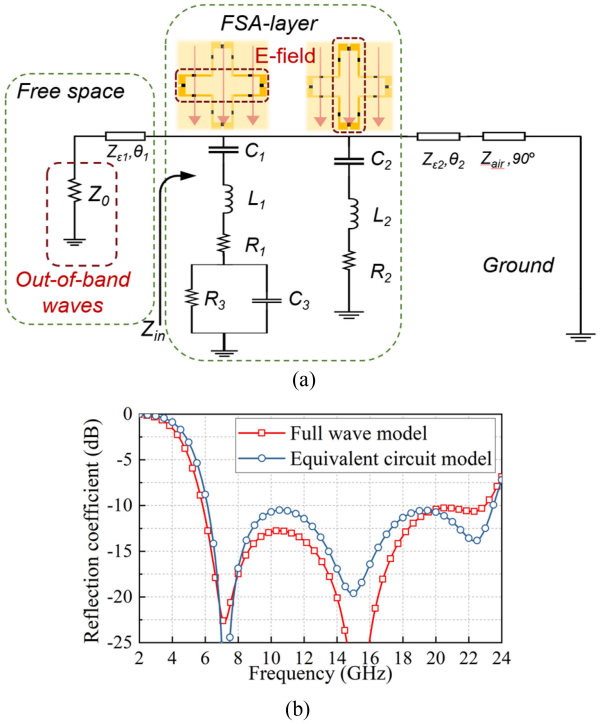

FIGURE 8. (a) Equivalent circuit model of the FSA-layer, (b) Reflection coefficients of ECM and full wave model. (Circuit parameters: $C_1 = 0.045$ pF, $L_1 = 0.24$ nH, $R_1 = 240$ Ω, $C_2 = 0.045$ pF, $L_2 = 0.24$ nH, $R_2 = 240$ Ω, $C_3 = 0.045$ pF, $R_3 = 240$ Ω, $Z_{\varepsilon 2} = 80$, $\theta_2 = 90$, $Z_{air} = 377$).

$$G_2 = \frac{R_2}{R_2^2 + \left(\omega L_2 - \frac{1}{\omega C_2}\right)^2} \tag{10}$$

$$B_2 = \frac{\omega L_2 - \frac{1}{\omega C_2}}{R_2^2 + \left(\omega L_2 - \frac{1}{\omega C_2}\right)^2} \tag{11}$$

In the overall ECM model, the condition for achieving circuit matching is $Y_{in} - Y_0 = Y_1 + Y_2 + Y_d = 0$, when the sum of imaginary parts is equal to zero ($B_1 + B_2 + B_d = 0$). The reflection coefficient results are optimized through ADS simulations, along with the calculation of corresponding circuit parameters. By confirming the optimal value of circuit parameters, the reflection coefficient result of ECM is shown in Fig. 8 (b). It achieves three resonances within the operating frequency band, which is consistent with the result of the full wave simulation. Thus, it can be anticipated that the hybrid FSA, combining the two structures of antenna-based absorber and FSA-layer, has the possibility to simultaneously achieve both in-band and out-of-band absorption.

V. DESIGN OF THE INTEGRATED STRUCTURE

A. UNIT CELL OF THE HYBRID FSA

Fig. 9 shows the model and simulated results of the proposed hybrid FSA (Antenna-based FSA & FSA-layer) at the boundary conditions of the unit cell. As shown in Fig. 9 (a), the patterns of the patch-layer and the FSA-layer are complementary to each other to ensure their independent operation and compatibility with subsequent installation. Fig. 9 (b) shows that the reflection coefficient is less than −10 dB over the frequency range of 3-23 GHz (FBW = 120%). Fig. 10 (a) presents that the reflection coefficients for different polarized incident waves are stable. It can be indicated

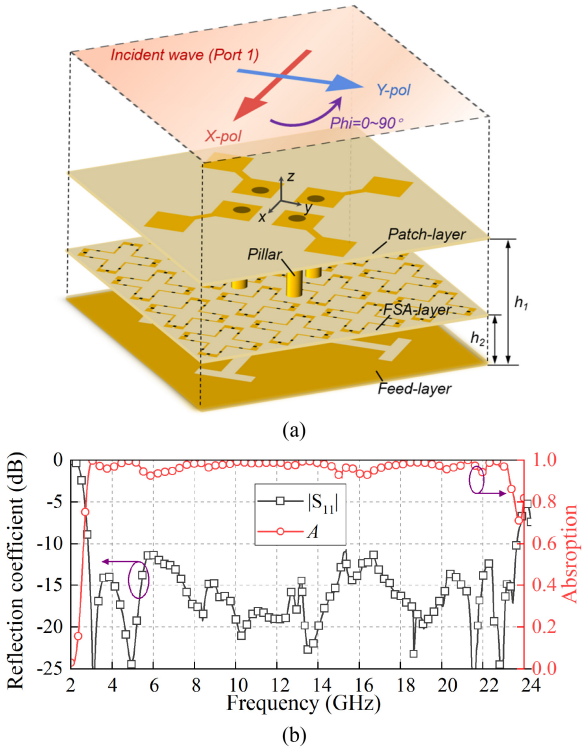

FIGURE 9. (a) Unit cell model the proposed hybrid FSA, (b) $|S_{11}|$ and absorption.

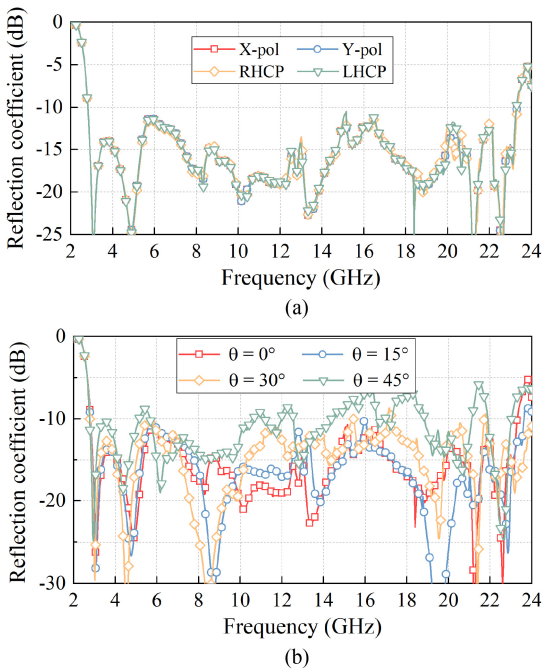

FIGURE 10. Simulated results of (a) reflection coefficients for different Phi incident waves, (b) reflection coefficients for different oblique incidence.

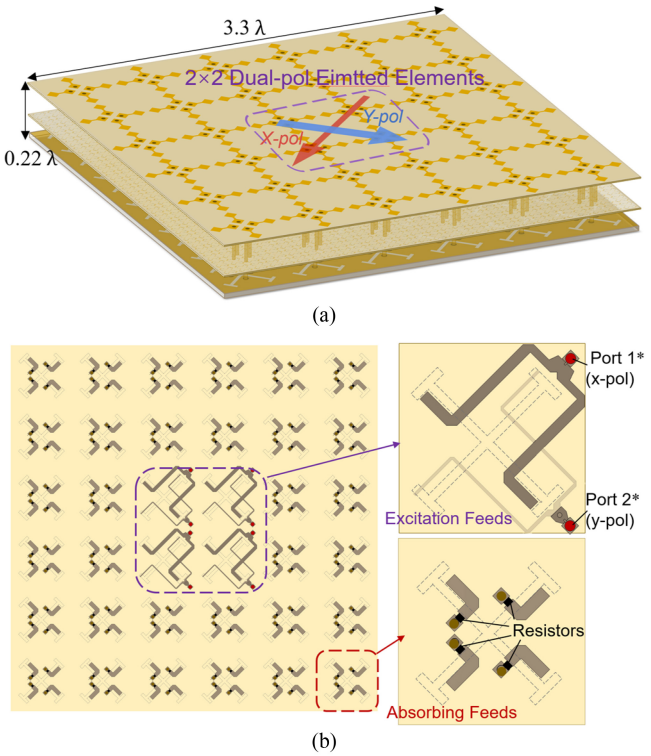

FIGURE 11. Geometry of the hybrid FSA with antenna circuits. (a) 3D model, (b) bottom view and feeding network.

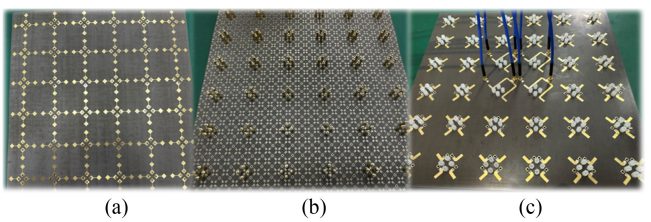

FIGURE 12. The prototype of the integrated structure. (a) Top view of the patch-layer, (b) Top view of the feed-layer, (c) Bottom view of the feed-layer.

that the proposed hybrid FSA has ultra-wideband absorption for any polarized incident wave. Moreover, the reflection coefficients under different oblique incidences ($\theta = 0°$, 15°, 30°, and 45°) are given in Fig. 10 (b). It can be noticed that the proposed antenna shows stable reflection coefficient when the oblique incidence is less than 30°. When the angle of incidence increases to 45°, the integrated structure may produce unnecessary resonances at higher frequency, leading to the occurrence of additional reflection.

B. THE INTEGRATED HYBRID FSA WITH ANTENNA CIRCUITS

Fig. 11 (a) presents the geometry of the integrated hybrid FSA with antenna circuits. The proposed structure is composed of 6 × 6 array elements. The overall size of the structure is $3.3\lambda_0 \times 3.3\lambda_0 \times 0.22\lambda_0$ (λ_0 is the wavelength at the center frequency of 4 GHz in free space). The structure is fixed by copper pillars and screws, securing

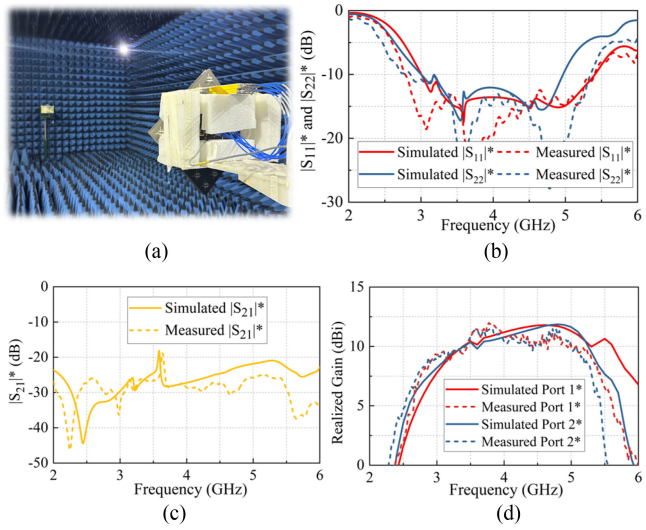

FIGURE 13. (a) Photograph of measurement, (b) Simulated and measured results of $|S_{11}|^*$ and $|S_{22}|^*$ for proposed structure, (c) $|S_{21}|^*$, (d) Realized gains of Port 1* and Port 2*.

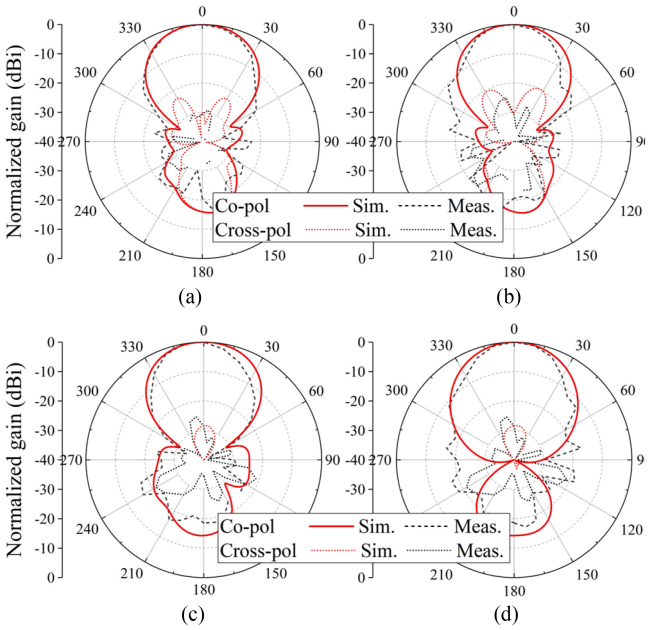

FIGURE 14. Simulated and measured radiation patterns of proposed structure at 4 GHz (a) *xoz*-plane of Port 1*, (b) *yoz*-plane of Port 1*, (c) *xoz*-plane of Port 2*, and (d) *yoz*-plane of Port 2*.

the patch-layer, FSA-layer, and feed-layer in sequence. It's worth noting that the structure can excite any number of elements. In this section, excitation feeding is applied to the central of 2×2 elements, with the x-polarization and y-polarization directions parallel to the diagonal of the model. In contrast to the previous circuit in Fig. 2 (d), the feed-layer in Fig. 11 (b) has an additional intermediate layer to separate the antenna feeding networks for x-polarization and y-polarization. As depicted in Fig. 11 (b), the central 2×2 dual-polarized elements are driven by two power dividers, individually. The feeding network for x-polarization

TABLE 1. Comparisons of various among FSA structure with antenna function.

Ref.	Structure with Antenna Circuits (Elements)	Polarization	Antenna Impedance FBW	Size ($\lambda_0\times\lambda_0\times\lambda_0$)	RCS Reduction FBW (10 dB, %)
[15] yr:2024	Frequency Selective Rasorbers with F-P antenna	LHCP	11.8-12.2 GHz, 3.3%	4.8×4.8×0.51	9.9-11.3 GHz and 13.3-20 GHz (53%).
[29] yr:2020	Hybrid Metasurface with Slot Array (4×4)	Single	9.5-10.2 GHz, 7.1%	2.2×2.2×0.8	6-18 GHz (100%)
[30] yr:2021	Hybrid Metasurface with Fed Fabry-Perot antenna	Single	9.2-10.6 GHz, 14.1%	2.6×2.0×0.9	8-19 GHz (81.5%)
[32] yr:2022	Reconfigurable Multilayer FSA with Patch Antenna (4×4)	Single	8.15-8.45 GHz, 3.6%	1.88×2.08×0.2	4.02-13.82 GHz (109.8%)
[39] yr:2021	Integrated Resistors Dipole Array (4×4)	LHCP	5.66-6.12 GHz, 7.8%	2.4×2.4×0.21	3-9.8 GHz (106%)
This work	Integrated hybrid FSA with antenna circuits (2×2)	**Dual**	**2.8-5.5 GHz, 65.06%**	**3.3×3.3×0.22**	**2.8-23 GHz (156.6%)**

Where f_0 is the center frequency of operating band of antenna and λ_0 is the corresponding wavelength **yr** is the year of publication

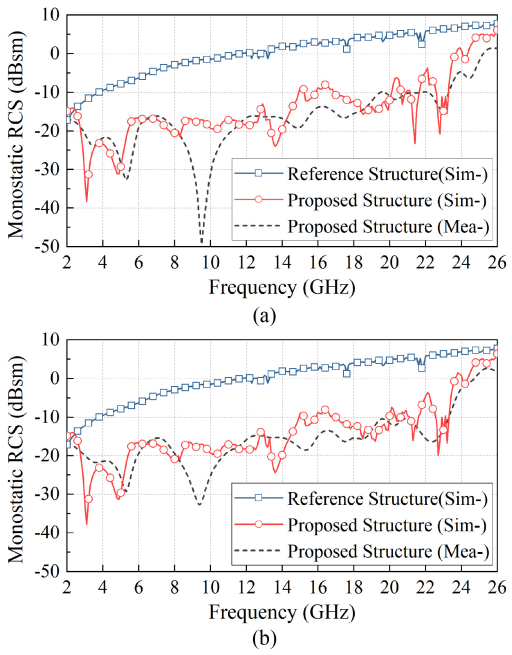

FIGURE 15. Simulated and measured monostatic RCS of integrated array. (a) x- and (b) y-polarization.

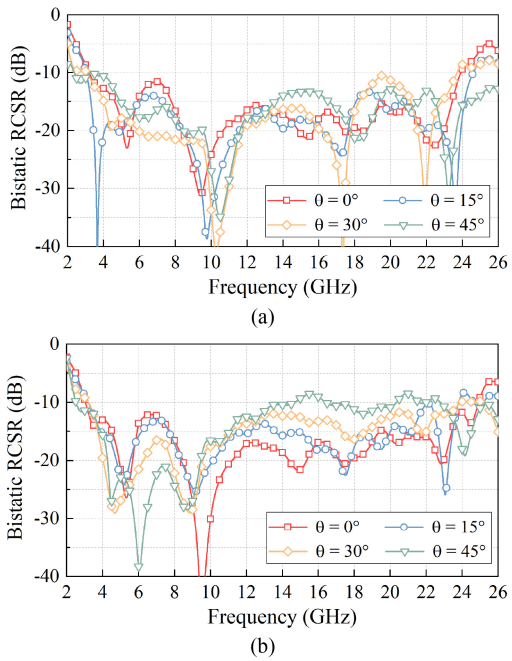

FIGURE 16. Measured basic RCSR of integrated array under different oblique incidences. (a) x- and (b) y-polarization.

is etched at the bottom of the feed-layer, connected to Port 1*. The feeding network for y-polarization is etched on the intermediate layer of the feed-layer, connected to Port 2*. Other elements beside the 2×2 antenna elements in the same layer are connected to absorption resistors, consistent with the circuit configuration in Fig. 2 (d).

VI. EXPERIMENT VERIFICATION

A. PROTOTYPE OF THE INTEGRATED STRUCTURE

To verify the feasibility, the prototype of the integrated structure is fabricated and presented in Fig. 12. As shown in Fig. 12 (c), The excitation ports of each 2×2 emitted elements are individually connected to power dividers, which are then linked to input Port 1* and Port 2* of the vector network analyzer (VNA). Fig. 13 (a) gives the photograph of the radiation measurement setup in an anechoic chamber.

B. RADIATION PERFORMANCE

Fig. 13 (b) illustrates the simulated and measured S-parameters of the proposed integrated structure. As shown in Fig. 13 (b), the simulated $|S_{11}|^*$ is below −10 dB for 3-5.5 GHz and the $|S_{22}|^*$ is below −10 dB for 3-5 GHz. The measured results closely match the simulated ones. The measured results indicate that the proposed structure has an antenna fractional bandwidth of 65.06% (2.8–5.5 GHz) for $|S_{11}|^*$ and $|S_{22}|^* < -10$ dB. A slight difference between the measured and simulated bandwidths can be attributed to deviations induced by the losses in the test cables

and the actual sample during measurement. Fig. 13 (c) shows the simulated and measured isolations between two ports. The simulated and measured $|S_{21}|$* are both below −15 dB, indicating good isolation performance for both polarizations (Port 1* and Port 2*). Fig. 13 (d) shows the realized gain of the proposed structure, which shows a nice consistent between simulated and measured results. The realized gains vary in a range from 8 to 12 dBi for both polarizations over the operating band. Fig. 14 gives radiation patterns of the dual-polarized integrated array at the center frequency of 4 GHz, respectively. A favorable concurrence between measured and simulated results is discernible upon comparison. And the dual-polarized radiation patterns of the proposed array exhibit consistent stability. In addition, cross-polarization levels in the xoz-plane and yoz-plane are consistently below −20 dB.

C. SCATTERING PERFORMANCE OF THE PROPOSED STRUCTURE

To show the effect of the proposed structure for RCS reduction, both the simulated and measured monostatic RCS of the proposed structure are investigated and compared with the reference structure. The reference antenna is a slot antenna array, which is the same as the feed-layer of the proposed antenna. The measurements are also conducted in an anechoic chamber, with the prototype structure positioned vertically on a foam platform and terminated with a matched load of 50 Ω. Fig. 15 (a) and (b) respectively depicts the monostatic RCS results for x- and y-polarized normally incident waves, both in measured and simulated forms. Remarkably, the measured RCS values of the proposed structure exhibit excellent agreement with the simulated ones. For the x-polarized incidence, the RCS reduction (RCSR) of 10 dB is observed ranging from 2.8 to 23 GHz with the FBW of 81.5%, and it is consistent for the y-polarization. It indicates the proposed structure achieves the ultra-wideband low RCS performance for both of x- and y-polarizations. It can be mentioned that the measured RCSR of the proposed structure relative to a perfect electric conductor (PEC) of the same size is as follows [34]:

$$RCSR = RCS_{structure} - RCS_{pec} = 10\log_{10}\frac{P_s}{P_i} \quad (12)$$

where Ps represents the scattered power per area of the target, and Pi represents the incident power per area of the target. Furthermore, the reflection coefficient can also be expressed by the formula [40]:

$$|R_i|^2 = \frac{P_s}{P_i} \quad (13)$$

where *Ri* represents the reflection coefficient for the incident wave. Thus, these calculations allow for the equivalence between the reflection coefficient and RCSR. To verify the scattering performance under various oblique incidences, the bistatic RCSR of the proposed structure is conversed by measured reflection coefficients and presented in Fig. 16. It can be noticed that the proposed structure shows stable RCSR when the oblique incidence is less than 30° under both x- and y-polarization (TM and TE modes for incident waves). and λ_0 is the corresponding wavelength, yr: year of publication.

To better understand the attractive advantages of the proposed structure, a comparative study with other reported is tabulated in Table 1. The comparison with other reported works has validated the effectiveness of the proposed structure in design of RCSR. the proposed structure has the widest RCSR FBW of 156.6%, the widest dual-polarized radiation performance FBW of 65.06%, and comparable low profile of $0.22\lambda_0$.

VII. CONCLUSION

In this paper, an integrated hybrid FSA with antenna circuits is proposed and fabricated to realize wideband dual-polarized radiations and ultra-wideband absorption. The novel design features an integrating antenna-based absorber arrays enabling the structure to receive incoming waves and subsequently absorb them at the feeding port. The proposed structure involves utilizing center arrays as emitted elements, while remaining arrays serving as absorbing elements. Additionally, the structure integrates the FSA-layer to reduce out-of-band RCS without affecting the in-band performance. The measured results demonstrate that the proposed structure has broadband antenna impedance bandwidth and ultra-wideband RCS reduction when it compares with reported works. In summary, this versatile design offers promising applications in radar systems, communication devices, and low observable platforms, making it an asset in electromagnetic engineering.

REFERENCES

[1] J. W. You, J. F. Zhang, W. X. Jiang, H. F. Ma, W. Z. Cui, and T. J. Cui, "Accurate analysis of finite-volume lumped elements in metamaterial absorber design," *IEEE Trans. Microw. Theory Tech.*, vol. 64, no. 7, pp. 1966–1975, Jul. 2016.

[2] J. Lee, M. Yoo, and S. Lim, "A study of ultra-thin single layer frequency selective surface microwave absorbers with three different bandwidths using double resonance," *IEEE Trans. Antennas Propag.*, vol. 63, no. 1, pp. 221–230, Jan. 2015.

[3] H. T. Liu, H. F. Cheng, Z. Y. Chu, and D. Y. Zhang, "Absorbing properties of frequency selective surface absorbers with cross-shaped resistive patches," *Mater. Design*, vol. 28, no. 7, pp. 2166–2171, 2007.

[4] E. F. Knott, J. F. Shaeffer, and M. T. Tuley, *Radar Cross Section*. Stevenage, U.K.: SciTech, 2004.

[5] L. J. Du Toit, "The design of Jauman absorbers," *IEEE Antennas Propag. Mag.*, vol. 36, no. 6, pp. 17–25, Dec. 1994.

[6] L. J. Du Toit and J. H. Cloete, "Electric screen Jauman absorber design algorithms," *IEEE Trans. Microw. Theory Tech.*, vol. 44, no. 12, pp. 2238–2245, Dec. 1996.

[7] B. A. Munk, P. Munk, and J. Pryor, "On designing Jaumann and circuit analog absorbers (CA absorbers) for oblique angle of incidence," *IEEE Trans. Antennas Propag.*, vol. 55, no. 1, pp. 186–193, Jan. 2007.

[8] Y. Shang, Z. Shen, and S. Xiao, "On the design of single-layer circuit analog absorber using double-square-loop array," *IEEE Trans. Antennas Propag.*, vol. 61, no. 12, pp. 6022–6029, Dec. 2013.

[9] A. P. Sohrab and Z. Atlasbaf, "A circuit analog absorber with optimum thickness and response in X-band," *IEEE Antennas Wireless Propag. Lett.*, vol. 12, pp. 276–279, 2013.

[10] J. Chen, Y. Shang, and C. Liao, "Double-layer circuit analog absorbers based on resistor-loaded square-loop arrays," *IEEE Antennas Wireless Propag. Lett.*, vol. 17, no. 4, pp. 591–595, Apr. 2018.

[11] Z. Ma, C. Jiang, W. Cao, J. Li, and X. Huang, "An ultrawideband and high-absorption circuit-analog absorber with incident angle-insensitive performance," *IEEE Trans. Antennas Propag.*, vol. 70, no. 10, pp. 9376–9384, Oct. 2022.
[12] H. Li et al., "Phase-loss cascade combination method for multilayer ultrabroadband reconfigurable absorber," *IEEE Trans. Microw. Theory Tech.*, vol. 72, no. 4, pp. 2224–2233, Apr. 2024.
[13] G. Q. Luo, W. Yu, Y. Yu, X. H. Zhang, and Z. Shen, "A three-dimensional design of ultra-wideband microwave absorbers," *IEEE Trans. Microw. Theory Tech.*, vol. 68, no. 10, pp. 4206–4215, Oct. 2020.
[14] B. Li and Z. Shen, "Wideband 3D frequency selective rasorber," *IEEE Trans. Antennas Propag.*, vol. 62, no. 12, pp. 6536–6541, Dec. 2014.
[15] S. Wang, H.-X. Xu, M. Wang, and S. Tang, "A Low-RCS, High-Gain and Polarization-Insensitive FP Antenna Combing Frequency Selective rasorber and metasurface," *IEEE Open J. Antennas Propag.*, early access, Jul. 25, 2024, doi: 10.1109/OJAP.2024.3426624.
[16] X. Q. Lin, P. Mei, P. C. Zhang, Z. Z. D. Chen, and Y. Fan, "Development of a resistor-loaded ultrawideband absorber with antenna reciprocity," *IEEE Trans. Antennas Propag.*, vol. 64, no. 11, pp. 4910–4913, Nov. 2016.
[17] M. S. Neiman, "The principle of reciprocity in antenna theory," *Proc. IRE*, vol. 31, no. 12, pp. 666–671, Dec. 1943.
[18] C. Wu, S. Lu, Z. Yang, and Y. Yashchyshyn, "A UWB absorber based on the TCA concept in the UHF band," *IEEE Trans. Antennas Propag.*, vol. 68, no. 5, pp. 4132–4136, May 2020.
[19] H. Jiang, S. Liao, J. Shen, and Q. Xue, "Receiving and transmitting antenna pairs based rasorber with high angular stability," *IEEE Trans. Microw. Theory Tech.*, vol. 71, no. 8, pp. 3235–3247, Aug. 2023.
[20] M. M. Zargar, A. Rajput, and K. Saurav, "Miniaturized design of dual transmission frequency selective rasorber with wide angular stability," *IEEE Open J. Antennas Propag.*, vol. 5, no. 4, pp. 922–932, Aug. 2024.
[21] Y. He, J. Jiang, M. Chen, S. Li, L. Miao, and S. Bie, "Design of an adjustable polarization-independent and wideband electromagnetic absorber," *J. Appl. Phys.*, vol. 119, no. 10, 2016, Art. no. 105103.
[22] S. Kim and S. Nam, "Ultra-wideband and wide-angle insensitive absorber based on TCDA-under-tightly coupled dipole array," *IEEE Trans. Antennas Propag.*, vol. 69, no. 9, pp. 5682–5690, Sep. 2021.
[23] Q. Chen, M. Guo, D. Sang, Z. Sun, and Y. Fu, "RCS reduction of patch array antenna using anisotropic resistive metasurface," *IEEE Antennas Wireless Propag. Lett.*, vol. 18, no. 6, pp. 1223–1227, Jun. 2019.
[24] Z. Sun, Q. Chen, M. Guo, and Y. Fu, "Low-RCS reflectarray antenna based on frequency selective rasorber," *IEEE Antennas Wireless Propag. Lett.*, vol. 18, no. 4, pp. 693–697, Apr. 2019.
[25] B. Zhang, Q. Lv, J. Chen, and Y. Tang, "Low-RCS and wideband reflectarray antenna with high radiation efficiency," *IEEE Trans. Antennas Propag.*, vol. 69, no. 7, pp. 4212–4216, Jul. 2021.
[26] W. Yu, Y. Yu, W. Wang, X. H. Zhang, and G. Q. Luo, "Low-RCS and gain-enhanced antenna using absorptive/transmissive frequency selective structure," *IEEE Trans. Antennas Propag.*, vol. 69, no. 11, pp. 7912–7917, Nov. 2021.
[27] J. Sun, Q. Cao, Y. Li, and H. Li, "Functional reconfigurable integrated structure of circularly polarized antenna and FSS absorber," *IEEE Trans. Antennas Propag.*, vol. 69, no. 11, pp. 7260–7268, Nov. 2021.
[28] Y. Han, L. Zhu, Y. Bo, W. Che, and B. Li, "Novel low-RCS circularly polarized antenna arrays via frequency-selective absorber," *IEEE Trans. Antennas Propag.*, vol. 68, no. 1, pp. 287–296, Jan. 2020.
[29] Y. Liu, Y. Jia, W. Zhang, and F. Li, "Wideband RCS reduction of a slot array antenna using a hybrid metasurface," *IEEE Trans. Antennas Propag.*, vol. 68, no. 5, pp. 3644–3652, May 2020.
[30] X. Liu, Z. Yan, E. Wang, T. Zhang, and F. Fan, "Magnetoelectric dipole-fed Fabry–Perot antenna with wideband RCS reduction based on multilayer metasurface," *IEEE Antennas Wireless Propag. Lett.*, vol. 20, pp. 1342–1346, 2021.
[31] M. Li, Z. Yi, Y. Luo, B. Muneer, and Q. Zhu, "A novel integrated switchable absorber and radiator," *IEEE Trans. Antennas Propag.*, vol. 64, no. 3, pp. 944–952, Mar. 2016.
[32] J. Sun, Q. Cao, M. Pan, and L. Zhu, "A broadband multilayer absorber with switchable function of radiation," *IEEE Trans. Antennas Propag.*, vol. 70, no. 8, pp. 6841–6849, Aug. 2022.
[33] K. N. Rozanov, "Ultimate thickness to bandwidth ratio of radar absorbers," *IEEE Trans. Antennas Propag.*, vol. 48, no. 8, pp. 1230–1234, Aug. 2000.
[34] S. Zheng, Y. Yin, J. Fan, X. Yang, B. Li, and W. Liu, "Analysis of miniature frequency selective surfaces based on fractal antenna–filter–antenna arrays," *IEEE Antennas Wireless Propag. Lett.*, vol. 11, pp. 240–243, 2012.
[35] N. I. Landy, S. Sajuyigbe, J. J. Mock, D. R. Smith, and W. J. Padilla, "Perfect metamaterial absorber," *Phys. Rev. Lett.*, vol. 100, no. 20, 2008, Art. no. 207402.
[36] H. Lin, Y. Li, S.-W. Wong, K. W. Tam, B. Liu, and L. Zhu, "High-selectivity FA-FA-based frequency selective surfaces using magnetoelectronic dipole antennas," *IEEE Trans. Antennas Propag.*, vol. 70, no. 11, pp. 10669–10677, Nov. 2022.
[37] L. Ge and K. M. Luk, "A low-profile magneto-electric dipole antenna," *IEEE Trans. Antennas Propag.*, vol. 60, no. 4, pp. 1684–1689, Apr. 2012.
[38] S. Ghosh and K. V. Srivastava, "An equivalent circuit model of FSS-based metamaterial absorber using coupled line theory," *IEEE Antennas Wireless Propag. Lett.*, vol. 14, pp. 511–514, 2015.
[39] C. Jin, B. Zhang, L. Yin, Q. Lv, L. Kong, and L. Li, "Integrated low-profile low radar cross section circularly polarized dipole antenna array," *IEEE Trans. Antennas Propag.*, vol. 69, no. 12, pp. 8461–8469, Dec. 2021.
[40] W. Hofmann, C. Bornkessel, A. Schwind, and M. A. Hein, "Challenges of RF absorber characterization: Comparison between RCS-and NRL-arch-methods," in *Proc. Int. Symp. Electromagn. Compat.-EMC EUROPE)*, 2019, pp. 370–375.

YOUQUAN WEN received the M.E. degree from Central South University, Hunan, China. He is currently pursuing the Ph.D. degree with the College of Electronics and Information Engineering, Shenzhen University, Guangdong, China.

His current research interests include radar cross section reduction of antennas, metasurfaces, magnetoelectric-dipole antenna, and antenna arrays.

SAI-WAI WONG (Senior Member, IEEE) received the B.S. degree in electronic engineering from the Hong Kong University of Science and Technology, Hong Kong, in 2003, and the M.Sc. and Ph.D. degrees in communication engineering from Nanyang Technological University, Singapore, in 2006 and 2009, respectively.

From July 2003 to July 2005, he was an Electronic Engineer to lead an electronic engineering department in China with two Hong Kong manufacturing companies. From May 2009 to October 2010, he was a Research Fellow with the ASTAR Institute for Infocomm Research, Singapore. Since 2010, he has been an Associate Professor and later become a Full Professor with the School of Electronic and Information Engineering, South China University of Technology, Guangzhou, China. Since 2017, he has been a tenured Full Professor with the College of Electronics and Information Engineering, Shenzhen University, Shenzhen, China. So far, he has authored and co-authored more than 300 papers in international journals and conference proceedings. He is the main inventor with more than 70 authorized Chinese Invention Patents. His current research interests include RF/microwave circuit and antenna design, and integrated sensing and communication. He was the recipient of the New Century Excellent Talents in University awarded by the Ministry of Education of China in 2013 and the Shenzhen Overseas High-Caliber Personnel Level C in 2018.

CHUNLIN JI received the M.Phil. degree from the University of Cambridge, Cambridge, U.K., in 2006, and the Ph.D. degree from Duke University, Durham, NC, USA, in 2009. He has been the Vice President and the Principle Scientist with the Kuang-Chi Institute of Advanced Technology, Shenzhen, China, since 2010. His current research interests include Bayesian statistics, data science, machine learning algorithms, and metamaterial design.

RUOPENG LIU received the Ph.D. degree from Duke University, Durham, NC, USA, in 2009. He has been the President of the Kuang-Chi Institute of Advanced Technology, Shenzhen, China, since 2010. His current research interests include resonance frequency, split-ring resonator, antenna array, and metamaterial structure.

YEJUN HE (Senior Member, IEEE) received the Ph.D. degree in information and communication engineering from the Huazhong University of Science and Technology (HUST), Wuhan, China, in 2005. From 2005 to 2006, he was a Research Associate with the Department of Electronic and Information Engineering, The Hong Kong Polytechnic University, Hong Kong. From 2006 to 2007, he was a Research Associate with the Department of Electronic Engineering, Faculty of Engineering, The Chinese University of Hong Kong, Hong Kong. In 2012, he joined the Department of Electrical and Computer Engineering, University of Waterloo, Waterloo, ON, Canada, as a Visiting Professor. From 2013 to 2015, he was an Advanced Visiting Scholar (Visiting Professor) with the School of Electrical and Computer Engineering, Georgia Institute of Technology, Atlanta, GA, USA. From 2023 to 2024, he was an Advanced Research Scholar (Visiting Professor) with the Department of Electrical and Computer Engineering, National University of Singapore, Singapore. Since 2006, he has been a Faculty with Shenzhen University, Shenzhen, China, where he is currently a Full Professor with the College of Electronics and Information Engineering, the Director of Sino-British Antennas and Propagation Joint Laboratory of Ministry of Science and Technology of the People's Republic of China (MOST), the Director of the Guangdong Engineering Research Center of Base Station Antennas and Propagation, and the Director of the Shenzhen Key Laboratory of Antennas and Propagation. He was selected as a Leading Talent in the "Guangdong Special Support Program" and the Shenzhen "Pengcheng Scholar" Distinguished Professor, China, in 2024 and 2020, respectively. He has authored or coauthored more than 300 refereed journal and conference papers and seven books. He holds about 20 patents. His research interests include wireless communications, antennas, and radio frequency.